Title	Investigation of electrical transport in anodized single TiO2 nanotubes
Author(s)	Hattori, Masashi; Noda, Kei; Nishi, Tatsuya; Kobayashi, Kei; Yamada, Hirofumi; Matsushige, Kazumi
Citation	Applied Physics Letters (2013), 102(4)
Issue Date	2013-01
URL	http://hdl.handle.net/2433/171148
Right	© 2013 American Institute of Physics
Type	Journal Article
Textversion	publisher

AIP | Applied Physics Letters

Investigation of electrical transport in anodized single TiO2 nanotubes

Masashi Hattori, Kei Noda, Tatsuya Nishi, Kei Kobayashi, Hirofumi Yamada et al.

Citation: Appl. Phys. Lett. **102**, 043105 (2013); doi: 10.1063/1.4789763
View online: http://dx.doi.org/10.1063/1.4789763
View Table of Contents: http://apl.aip.org/resource/1/APPLAB/v102/i4
Published by the American Institute of Physics.

Related Articles

An exact solution of the linearized Boltzmann transport equation and its application to mobility calculations in graphene bilayers
J. Appl. Phys. 113, 093702 (2013)

Disorder-tuned charge transport in organic semiconductors
APL: Org. Electron. Photonics 6, 39 (2013)

Disorder-tuned charge transport in organic semiconductors
Appl. Phys. Lett. 102, 083304 (2013)

Mechanism of dopant-vacancy association in α-quartz GeO2
J. Appl. Phys. 113, 083716 (2013)

Enhancement of multisubband electron mobility in parabolic AlxGa1−xAs-GaAs double quantum well structures
J. Appl. Phys. 113, 083704 (2013)

Additional information on Appl. Phys. Lett.

Journal Homepage: http://apl.aip.org/
Journal Information: http://apl.aip.org/about/about_the_journal
Top downloads: http://apl.aip.org/features/most_downloaded
Information for Authors: http://apl.aip.org/authors

ADVERTISEMENT

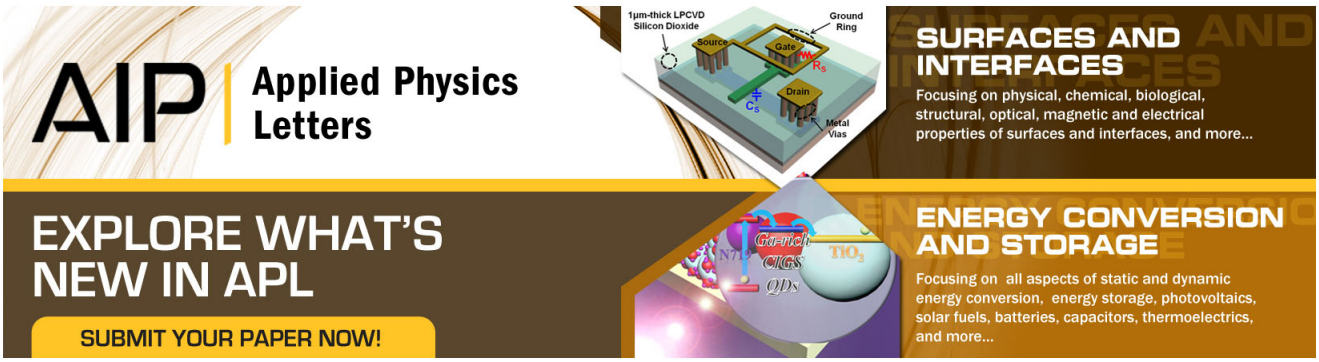

Investigation of electrical transport in anodized single TiO_2 nanotubes

Masashi Hattori,[1] Kei Noda,[1,a)] Tatsuya Nishi,[1] Kei Kobayashi,[2] Hirofumi Yamada,[1] and Kazumi Matsushige[3]
[1]*Department of Electronic Science and Engineering, Kyoto University, Katsura, Nishikyo, Kyoto 615-8510, Japan*
[2]*Office of Society-Academia Collaboration for Innovation, Kyoto University, Katsura, Nishikyo, Kyoto 615-8520, Japan*
[3]*Faculty of Science and Technology, Ryukoku University, 1-5 Yokotani, Setaoe-cho, Otsu, Shiga 520-2194, Japan*

(Received 9 November 2012; accepted 15 January 2013; published online 29 January 2013)

Electrical transport in anodized single titania nanotube (TNT) free from any structural effects of titania nanotube array (TNA) was investigated. An anodized TNA was disassembled into single TNTs with two-step anodization technique. Then, single TNT bridges between gold electrodes with a gap of 500 nm were prepared by dielectrophoretic alignment. Quantitative assessment of electron mobility inside single anatase and rutile TNT was carried out by 2-probe current-voltage measurement and analysis based on a metal-semiconductor-metal circuit model with Schottky barriers. Our approach to intrinsic electrical transport of single nanotube is quite effective for understanding the electronic and optical properties of TNA. © *2013 American Institute of Physics*. [http://dx.doi.org/10.1063/1.4789763]

Anodized titania (TiO_2) nanotube arrays (TNAs)[1–8] have attracted remarkable attention for diverse applications due to their unique combination of wide-band-gap semiconductor properties, nanotube geometry, and large surface area. Optical and electrical characteristics of TNAs, such as photoconversion efficiency[9] and carrier concentration,[10] have been intensely studied for understanding carrier behaviors inside TNAs and improving the performance of dye-sensitized solar cells and photocatalytic reactors based on TNAs. However, the relationship between individual titania nanotubes (TNTs) and their assembled objects, viz. TNA, in structural and physical properties has not been elucidated yet. In order to clarify this relationship, investigating electrical properties of single nanotubes is quite a difficult, but significant challenge.

In this work, we report a method to examine electrical transport properties of single anodized TNT. An anodized TNA was efficiently disassembled into single TNTs via two-step anodization technique. Successively, single TNT bridges over micro-scale electrodes were prepared by dielectrophoretic (DEP) alignment.[11,12] Quantitative evaluation of electron mobility inside single TNT was performed by 2-probe current-voltage measurements and analysis based on a metal-semiconductor-metal (M-S-M) circuit with Schottky barriers.[13–15] Finally, the difference in electron mobility and crystal structure for single anodized TNT will be discussed.

Single anodized TNTs were prepared by employing two-step anodization described hereinafter. TNAs were fabricated by anodizing Ti foils (100 μm-thick, Japan Metal Service) in a two-electrode electrochemical cell with titanium as anode and platinum as cathode, at a constant voltage across the electrodes. A 4:1 mixture of glycerol (99.0% purity, Nakaraitesk) and highly pure water (18.2 MΩ cm) containing 0.5 wt. % NH_4F (96.0% purity, Wako Pure Chemical Industries) was used as electrolyte. The anodizing potential and duration were 50 V and 10 h, respectively. Surface morphologies of the TNA were observed using a Hitachi S4500 scanning electron microscope (SEM). SEM images of an anodized Ti foil, represented in Fig. 1, clearly show that the TNA with 5 μm length and 200–250 nm pore size was formed under our experimental condition. After this primary anodization, the Ti foils were annealed in air for crystallization. In this study, three types of TNA were prepared by annealing under different conditions; non-annealed TNA, the TNA annealed at 723 K for 1 h, and the TNA annealed at 1073 K for 1 h. X-ray diffraction patterns (not shown here) indicate that crystal types of each sample were amorphous, anatase, and rutile, respectively. Then, these TNA specimens were anodized again using the same electrolyte as in the primary anodization for 30 min with a bias of 50 V. We confirmed with SEM observation that the TNA surface was not damaged after the second anodization of titanium foils.

The bottom side of the formed TNA was steadily connected with the Ti foil. However, the primary anodized TNA could be mechanically removed from the Ti foil probably because the second anodizing treatment made small pits on the bottom side of the TNA produced by the primary anodization. As a consequence, the TNA layer was disassembled

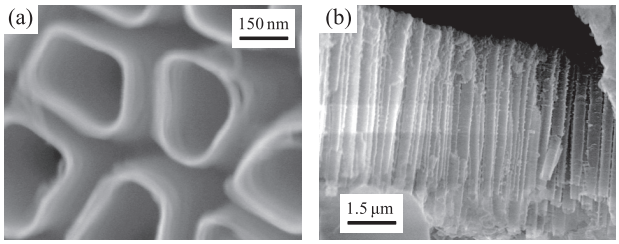

FIG. 1. SEM images of the TNA in (a) top view and (b) cross-sectional view.

a)Author to whom correspondence should be addressed. Electronic mail: nodakei@kuee.kyoto-u.ac.jp. Fax: +81-75-383-2308.

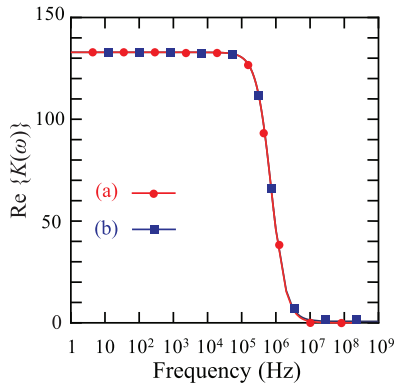

FIG. 2. The calculated Clausius-Mossotti factor of the (a) anatase and (b) rutile TNT.

into single TNTs with an average length of 1–2 μm by sonication in methanol.

Single TNT bridges between opposite gold (Au) electrodes with a gap of 500 nm were prepared by DEP alignment. The electrodes made of 3 nm-thick chromium (Cr) and 12 nm-thick Au were fabricated on heavily doped silicon (Si) substrates (size 1.5 cm × 1.5 cm) covered with a 300 nm-thick thermally grown SiO_2 by photolithography, vacuum evaporation, and successive lift-off process. The DEP assembly of TNTs was carried out as follows. A small droplet (5 μl) of the methanol solution of single TNTs was cast onto a Si substrate with 7 pairs of the electrodes. An AC voltage was applied with a function generator until the methanol droplet became dried off. The AC voltage gives rise to a time-averaged dielectrophoretic force given by[16–18]

$$F_{\mathrm{DEP}} \propto \varepsilon_{\mathrm{s}} \mathrm{Re}\{K(\omega)\} \nabla |E_{\mathrm{rms}}|^2, \tag{1}$$

$$\mathrm{Re}\{K(\omega)\} = \frac{1}{3} \frac{(\varepsilon_{\mathrm{p}} - \varepsilon_{\mathrm{s}})\{\varepsilon_{\mathrm{s}} + A(\varepsilon_{\mathrm{p}} - \varepsilon_{\mathrm{s}})\} + (\varepsilon'_{\mathrm{p}} - \varepsilon'_{\mathrm{s}})\{\varepsilon'_{\mathrm{s}} + A(\varepsilon'_{\mathrm{p}} - \varepsilon'_{\mathrm{s}})\}}{\{\varepsilon_{\mathrm{s}} + A(\varepsilon_{\mathrm{p}} - \varepsilon_{\mathrm{s}})\}^2 + \{\varepsilon'_{\mathrm{s}} + A(\varepsilon'_{\mathrm{p}} - \varepsilon'_{\mathrm{s}})\}^2}, \tag{2}$$

$$\varepsilon'_{\mathrm{p,s}} = \frac{\sigma_{\mathrm{p,s}}}{\varepsilon_0 \omega}, \tag{3}$$

where E_{rms} is the average electric field strength, ε_{p} and ε_{s} are the dielectric permittivity of the TNT and methanol, respectively, $K(\omega)$ is the Clausius-Mossotti (CM) factor, A is the depolarizing factor, σ is the conductivity, and $\omega = 2\pi f$ is the frequency of the applied AC voltage. Real parts of the CM factor calculated from Eq. (2) were shown in Fig. 2. In this calculation, $\varepsilon_{\mathrm{p}} = 31\varepsilon_0$, $\sigma_{\mathrm{p}} = 0.5$ S/m for anatase TNT; $\varepsilon_{\mathrm{p}} = 100\varepsilon_0$, $\sigma_{\mathrm{p}} = 0.5$ S/m for rutile TNT;[19–21] and $\varepsilon_{\mathrm{s}} = 31.2\varepsilon_0$, $\sigma_{\mathrm{s}} = 5.8 \times 10^{-4}$ S/m for methanol were given. As shown in Fig. 2, the frequency dependences of $\mathrm{Re}\{K(\omega)\}$ for anatase and rutile TNTs are almost same and the $\mathrm{Re}\{K(\omega)\}$ value is rapidly decreased when the frequency of the applied AC voltage increases from 100 kHz to 1 MHz. For the purpose of bridging only a single TNT between the contact electrodes, the amplitude and frequency of the AC voltage for the DEP alignment were chosen to be 6 $V_{p\text{-}p}$ and 0.5–1.0 MHz, respectively.

SEM images in Fig. 3 show that one or a few single TNTs were bridged over 500 nm gap between electrodes, suggesting that the dielectrophoretic alignment of various TNTs including amorphous, anatase, and rutile-type is feasible under our experimental conditions. Current-voltage (I–V) curves for these single TNT specimens were obtained with 2-point electrical measurement in a vacuum of 10^{-2} Pa

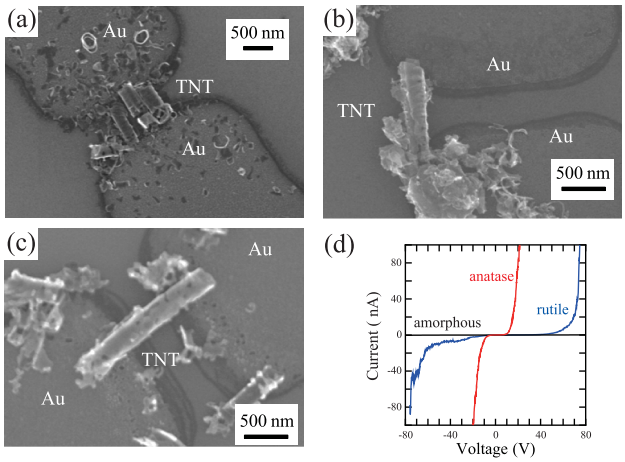

FIG. 3. SEM images of the single TNT bridging between the electrodes; (a) amorphous, (b) anatase, and (c) rutile TNT. (d) The current(I)-voltage(V) curves of each TNT.

under dark condition using a Keithley 4200-SCS system. As shown in Fig. 3(d), the current for the anatase and rutile TNTs were much larger than that for the amorphous TNT

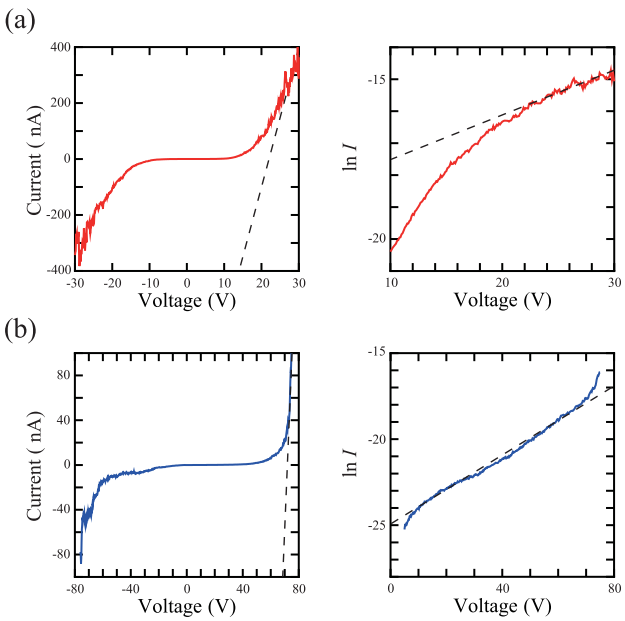

FIG. 4. I–V curves and their semi-logarithmic plots for the single (a) anatase and (b) rutile TNT. The dashed lines are the results best-fitted for I–V and ln(I)-V curves at higher voltages.

TABLE I. Physical parameters obtained from the experimental *I–V* curve.

	E_0 (meV)	Resistance (MΩ)	Resistivity (Ω cm)	Carrier concentration (cm^{-3})	Mobility ($cm^2/(Vs)$)
Anatase	26.0	19.5	10.2	1.7×10^{17}	3.6
Rutile	25.9	32.7	17.2	4.6×10^{18}	0.08

possibly due to high crystallinity of both anatase and rutile TNTs, and the current for the anatase TNT showed the largest value. These results are in line with prior data on the electrical conductivity of anodized TNAs annealed at different temperatures.[22] The obtained *I–V* curves for the anatase and rutile samples display nonlinear and symmetric curves, suggesting a semiconducting behavior of single TNT. Because the work function of Au (~5.1 eV) is higher than the conduction band levels of anatase and rutile TiO_2 and they behave as n-type semiconductors, the two contacts could be considered to be Schottky type. Therefore, the observed *I–V* characteristics should be modeled as M-S-M circuit with Schottky barriers.

The semiconductor parameters can be retrieved from the *I–V* data (Fig. 3) in the intermediate bias regime where the reverse-biased Schottky barrier dominates the total current *I*[13–15]

$$\ln I = \ln(SJ) = \ln S + V(q/kT - 1/E_0) + \ln J_s, \quad (4)$$

where J is the current density through the Schottky barrier, S is the contact area associated with this barrier, J_s is a slowly varying function of applied bias, q is the elementary charge, k is the Boltzmann constant, and E_0 is a parameter given by the equation: $E_0 = E_{00}\coth(E_{00}/kT)$, where $E_{00} = (\hbar q/2)(n/m^*\varepsilon)^{1/2}$. Here, n is the electron concentration, m^* is the effective electron mass, and ε is the permittivity of the TNT. According to Eq. (4), the logarithmic plot of the current I as a function of the bias V gives a straight line with a slope of $q/kT - 1/E_0$ as depicted in Fig. 4. Thus, the electron concentration n can be acquired via E_0, and the carrier mobility μ can be obtained from the following relationship: $\mu = 1/nq\rho$, with ρ being the resistivity of the TNT. Here, the resistance R for the TNT was determined by using linear characteristics of the *I–V* data in the regions of large bias ($R \sim dV/dI$). This is because, in this large bias regime, the voltages on the Schottky barriers are negligible compared to the voltage on the TNT and the applied voltage (V) is approximately equal to the voltage on the TNT. This series of analysis was utilized to investigate electron transport of compound semiconductor nanostructures such as zinc oxide nanowire[13] and boron nitride nanotube.[14]

TABLE II. Parameters used for obtaining electron mobility of single TNT.

	Anatase	Rutile
Electron effective mass	$1m_e$	$10m_e$
Dielectric permittivity	$31\varepsilon_0$	$100\varepsilon_0$
Temperature	300 K	300 K
Outer diameter of nanotube	200 nm	200 nm
Inner diameter of nanotube	180 nm	180 nm

Based on these procedures, the resistance, the resistivity, the carrier concentration, and the carrier mobility of the anatase and rutile TNT were extracted as summarized in Table I. Here, the parameters shown in Table II were used for obtaining these values. The derived mobility of the anatase (3.6 $cm^2/(Vs)$) and rutile (0.08 $cm^2/(Vs)$) TNT are in good agreement with those of the anatase and rutile TiO_2 polycrystalline thin films,[19] respectively. This derived anatase TNT mobility is about 1000 times larger than that of anatase TiO_2 nanoparticle films ($\leq 10^{-3}$ $cm^2/(Vs)$).[23] However, in a previous study of dye-sensitized TiO_2 solar cells (DSSCs) with intensity-modulated photocurrent spectroscopy (IMPS), the electron transport times of TiO_2 nanotube arrays and nanoparticle films were comparable.[24,25] This means that electron transport in TNA is interfered with some form of disorder. For example, formation of bundled TNT can affect electron transport dynamics in TNA.[25] Intertube-contacts within bundled TNT cause many electron pathways and make electron transport complicated in TNA. Eventually, the effective electron mobility of TNA becomes much lower than that of single TNT. This result shows that our approach to electrical properties of single nanotube is quite helpful in full comprehension of macroscopic characteristics of TNA.

Moreover, the estimated electron mobilities of the anatase and rutile TNT were largely different. This large difference can be useful for understanding the electronic and optical properties of TNA reported previously. For example, pure anatase TNA showed better photocatalytic properties compared to the mixture of anatase and rutile TNA.[26] It can be expected that lower electron mobility of photocatalysts gives rise to higher recombination rate of photogenerated electrons and holes, leading to the suppression of photocatalytic activity. Thus, the presence of rutile crystals in the mixture TNA causes poorer photocatalytic activity.

In conclusion, the electrical transport properties of individual anodized TNTs were investigated by using two-step anodization and dielectrophoretic alignment techniques. By analyzing measured current-voltage curves based on a M-S-M circuit model, the electron mobility of the single anatase and rutile TNT was evaluated to be 3.6 $cm^2/(Vs)$ and 0.08 $cm^2/(Vs)$, respectively. By using this method, the intrinsic electron mobility of TNT free from any structural effects of TNA can be estimated. To date, nanotubular oxide semiconductor photocatalysts, such as tantalum pentoxide (Ta_2O_5)[27] and tungsten trioxide (WO_3)[28] have been studied strenuously. Therefore, the characterization method for electrical transport reported in this work can contribute to the progress in understanding of basic electronic properties and materials development of these nanostructured photocatalysts.

This work was partly supported by Global Center of Excellence (G-COE) program of the Ministry of Education, Culture, Sports, Science, and Technology of Japan.

[1]J. M. Macak, H. Tsuchiya, L. Taveira, S. Aldabergerova, and P. Schmuki, Angew. Chem., Int. Ed. **44**, 7463 (2005).
[2]J. H. Park, O. O. Park, and S. Kim, Appl. Phys. Lett. **89**, 163106 (2006).
[3]Y. Hou, X. Y. Li, Q. D. Zhao, X. Quan, and G. H. Chen, Appl. Phys. Lett. **95**, 093108 (2009).
[4]M. Adachi, Y. Murata, M. Harada, and Y. Yoshikawa, Chem. Lett. **29**, 942 (2000).

[5]S. Z. Chu, S. Inoue, K. Wada, D. Li, H. Haneda, and S. Awatsu, J. Phys. Chem. B **107**, 6586 (2003).
[6]O. K. Varghese, M. Paulose, and C. A. Grimes, Nat. Nanotechnol. **4**, 592 (2009).
[7]Q. Chen and D. Xu, J. Phys. Chem. C **113**, 6310 (2009).
[8]M. Hattori, K. Noda, and K. Matsushige, Appl. Phys. Lett. **99**, 123107 (2011).
[9]C. Ruan, M. Paulose, O. K. Varghese, G. K. Mor, and C. A. Grimes, J. Phys. Chem. B **109**, 15754 (2005).
[10]F. Fabregat-Santiago, E. M. Barea, J. Bisquert, and G. K. Mor, J. Am. Chem. Soc. **130**, 11312 (2008).
[11]Y. Miyato, K. Kobayashi, K. Matsushige, and H. Yamada, Jpn. J. Appl. Phys., Part 1 **44**, 1633 (2005).
[12]J. Li, Q. Zhang, N. Peng, and Q. Zhu, Appl. Phys. Lett. **86**, 153116 (2005).
[13]Z. Y. Zhang, C. H. Jin, X. L. Liang, Q. Chen, and L.-M. Peng, Appl. Phys. Lett. **88**, 073102 (2006).
[14]X. Bai, D. Golberg, Y. Bando, C. Zhi, C. Tang, M. Mitome, and K. Kurashima, Nano Lett. **7**, 632 (2007).
[15]F. A. Padovani and R. Stratton, Solid-State Electron. **9**, 695 (1966).
[16]T. B. Jones, *Electromechanics of Particles* (Cambridge University Press, Cambridge, 1995).
[17]H. Morgan and N. G. Green, J. Electrost. **42**, 279 (1997).
[18]M. Castellarnau, A. Errachid, C. Madrid, A. Juarez, and J. Samitier, Biophys. J. **91**, 3937 (2006).
[19]H. Tang, K. Prasad, R. Sanjines, P. E. Schmid, and F. Levy, J. Appl. Phys. **75**, 2042 (1994).
[20]T. Miyata, S. Tsukada, and T. Minami, Thin Solid Films **496**, 136 (2006).
[21]M. K. Nowotny, T. Bak, and J. Nowotny, J. Phys. Chem. B **110**, 16270 (2006).
[22]A. Tighineanu, T. Ruff, S. Albu, R. Hahn, and P. Schmuki, Chem. Phys. Lett. **494**, 260 (2010).
[23]K. Yu and J. Chen, Nanoscale Res. Lett. **4**, 1 (2009).
[24]K. Zhu, N. R. Neale, A. Miedaner, and A. J. Frank, Nano Lett. **7**, 69 (2007).
[25]K. Zhu, T. B. Vinzant, N. R. Neale, and A. J. Frank, Nano Lett. **7**, 3739 (2007).
[26]S. Sreekantan, R. Hazan, and Z. Lockman, Thin Solid Films **518**, 16 (2009).
[27]N. K. Allam, X. J. Feng, and C. A. Grimes, Chem. Mater. **20**, 6477 (2008).
[28]R. Hahn, J. M. Macak, and P. Schmuki, Electrochem. Commun. **9**, 947 (2007).